Comparison of Two Simple Models for High Frequency Friction: Exponential versus Gaussian Wings†

Steven A. Adelman*

Department of Chemistry, Purdue University, West Lafayette, Indiana 47907-2084

Received: July 23, 2008; Revised Manuscript Received: January 12, 2009

Liquid phase vibrational energy relaxation (VER) times T_1 typically depend critically on the relaxing mode's high frequency friction or *wing function*. The wing function may, in principle, be found from the mode's normalized force autocorrelation function (faf) $C(t)$, since it is proportional to $\lim_{\omega\to\infty} \int_0^\infty \cos \omega t\, C(t)\, dt$. However, the full form of $C(t)$ is never available. Thus, the wing function is typically estimated from a *model faf* $C_M(t)$ which duplicates the known part of $C(t)$ and which (hopefully) approximates its unknown part with enough realism to yield meaningful $\omega \to \infty$ behavior. Unfortunately, apparently realistic $C_M(t)$'s can predict unphysical wing functions, and T_1's in error by tens of orders of magnitude. Thus, a condition is needed to discriminate between $C_M(t)$'s which yield meaningful and unphysical forms for the high frequency friction. This condition is shown to be that model faf's $C_M(t)$ yield physical wing functions if and only if these functions derive from the short time "heads" of the faf's. This test is applied to the model faf's $C_{ga}(t) \equiv \exp[-{}^1/_2(t/\tau)^2]$ and $C_{se}(t) \equiv \mathrm{sech}(t/\tau)$. These faf's cannot both be physical, since they yield incompatible Gaussian and exponential wing functions. The test accepts $C_{ga}(t)$ as physical. It, however, rejects $C_{se}(t)$, since its "tail" $\lim_{t\to\infty} C_{se}(t) = 2\exp(-t/\tau)$ (because of its long range) dominates the wing function.

I. Introduction

Liquid phase vibrational energy relaxation (VER) rates[1] depend critically on the parameter $\beta(\omega_\ell)$,which is the friction kernel $\beta(\omega)$ of the relaxing mode, evaluated at the mode's liquid phase frequency ω_ℓ. For example, in the simplest approximation,[2] the VER time T_1 is just

$$T_1 = \beta^{-1}(\omega_\ell) \tag{1.1}$$

Central to this paper, as illustrated in Figure 1, is *that typical* ω_ℓ*'s*[3] *overlap the high frequency wing region of* $\beta(\omega)$. Consequently, meaningful evaluations of T_1 require a realistic form for the high frequency friction or *wing function* $\lim_{\omega\to\infty} \beta(\omega)$.

Unfortunately, little is yet known about the exact mathematical form of $\lim_{\omega\to\infty} \beta(\omega)$.

Thus, so far in T_1 determinations,[2,4,5] wing function models have been adopted, without rigorous justification, on the basis of "reasonableness".

One convenient way of building such models is based on the proportionality of $\beta(\omega)$ to the Fourier transform of the mode's force autocorrelation function (faf)[6]

$$C(t) = \frac{\langle \tilde{\mathscr{F}}(t)\tilde{\mathscr{F}}\rangle_0}{\langle \tilde{\mathscr{F}}^2\rangle_0} \tag{1.2}$$

Specifically, one constructs "reasonable" *model faf's* $C_M(t)$, like those in Figures 2 and 3. One then justifies the corresponding wing function models on the basis of the "reasonableness" of the $C_M(t)$'s. (Models are required, since the full form of $C[t]$ is never available.)

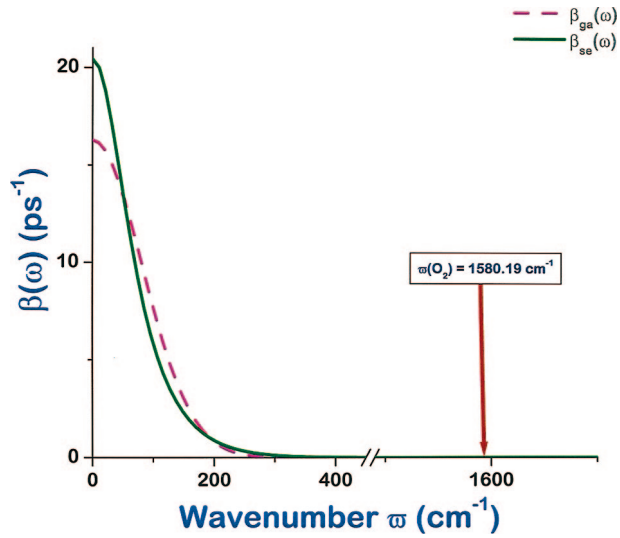

Figure 1. The model frequency dependent friction kernels $\beta_{ga}(\omega)$ (dashed curve) and $\beta_{se}(\omega)$ (solid curve) computed from eqs 1.4, 2.6, 2.7, and 2.10. The two kernels while of the same order of magnitude at low $\tilde{\omega}$, from eqs 2.8 and 2.9 and Table 3B, differ radically in the small amplitude wing function regime $\tilde{\omega} > 200$ cm^{-1} important for liquid phase VER.

The drawback of this method is that faf's which appear "reasonable" can yield unphysical wing functions, and, as illustrated in Table 1, *T_1's in error by tens of orders of magnitude*.

Figure 3 illustrates this point in a graphic manner. There we define and plot the model faf's $C_{gt}(t)$ and $C_{ms}(t)$. These certainly appear "reasonable". More strikingly, the two faf's also appear very similar. In fact, they are *nearly identical* well into their small amplitude long time "tail" regions.

† Originally submitted for the "Attila Szabo Festschrift", published as the May 15, 2008, issue of *J. Phys. Chem. B* (Vol. 112, No. 19).

* Phone: (765) 494-5277. Fax: (765) 494-0239. E-mail: saa@purdue.edu.

10.1021/jp806560x CCC: $40.75
Published on Web 03/26/2009

TABLE 1: VER Times $T_{1,ga} = \beta_{ga}^{-1}(\omega)$ and $T_{1,se} = \beta_{se}^{-1}(\omega)$ Computed from the Model faf's $C_{ga}(t)$ and $C_{se}(t)$ via eqs 1.4, 2.6, 2.7, and 2.10[a]

ω (fs^{-1})	ϖ (cm^{-1})	$T_{1,ga}$	$T_{1,se}$
0.02	106.18 (~K_2)	0.14 ps	0.19 ps
0.03	159.27 (~Na_2)	0.41 ps	0.52 ps
0.04	212.35 (~I_2)	1.80 ps	1.45 ps
0.05	265.44 (~I Br)	12.07 ps	4.04 ps
0.06	318.53 (~Br_2)	0.12 ns	11.21 ps
0.08	424.71 (~PbS)	45.67 ns	86.35 ps
0.1	530.88 (~SiCl)	91.72 μs	0.67 ns
0.12	637.06 (~ZnF)	1.00 s	5.13 ns
0.15	796.33 (~F_2)	2.69×10^7 s	0.11 μs
0.2	1061.77 (~LiH)	3.06×10^{23} s	18.09 μs
0.3	1592.65 (~O_2)	2.28×10^{69} s	0.49 s

[a] For $\tilde{\omega} < 200$ cm^{-1}, $T_{1,ga}$ and $T_{1,se}$ are similar. However, for $\tilde{\omega} \gtrsim 200$ cm^{-1}, $T_{1,ga}$ and $T_{1,se}$ diverge to eventually become radically different. As shown in the text, only $C_{ga}(t)$ is physical, and thus, the divergence arises because $\lim_{\omega\to\infty} \beta_{se}(\omega)$ has an unphysical form.

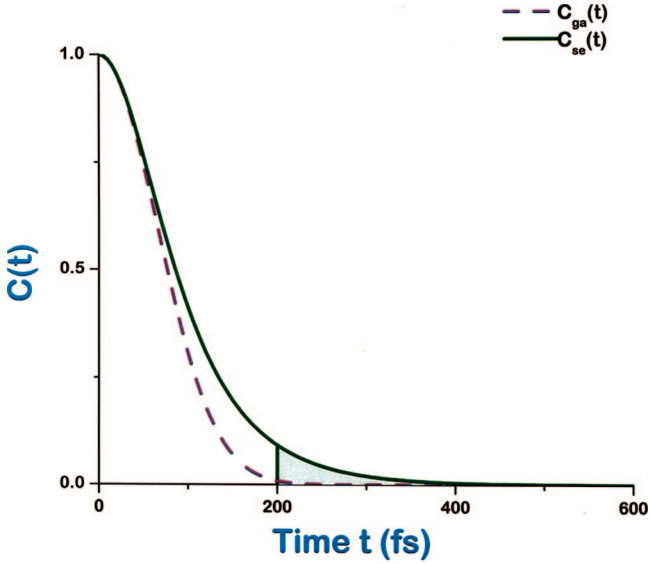

Figure 2. The model faf's $C_{ga}(t)$ (dashed curve) and $C_{se}(t)$ (solid curve) computed from eqs 2.4, 2.5, and 2.10. The $t < 200$ fs head parts of both faf's are of comparable magnitude and slope and thus make similar rapidly decaying contributions to the wing function. The $t > 200$ fs tail part of $C_{se}(t)$ (curve above shaded area) dominates $\beta_{se}(\omega)$ at high ω, giving rise to the exponential wing function of eq 2.9.

Given these features, one might expect that both faf's yield physical wing function models which, moreover, are very similar. However, from the caption of Figure 3, $C_{gt}(t)$ and $C_{ms}(t)$ actually predict *incompatible wing functions*, of, respectively, Gaussian and exponential form. This incompatibility, moreover, shows that at least one of the two model faf's yields an unphysical wing function (and thus must be rejected for VER).

We will soon see that similar comments apply to the model faf's of Figure 2.

Thus, the "reasonableness" of faf plots like those in Figures 2 and 3 can be very deceptive, and something more penetrating than inspection of such plots is needed to select faf's which are physical for VER and reject those which are not.

In other words, to advance beyond eq 1.1 and similar formal results,[4,5] the following problem is inescapable. *Find rigorous conditions which distinguish between faf's which predict physical and unphysical high frequency behavior.*

Elsewhere,[7] we deal with this problem in a general manner. Our central results are the following conditions.

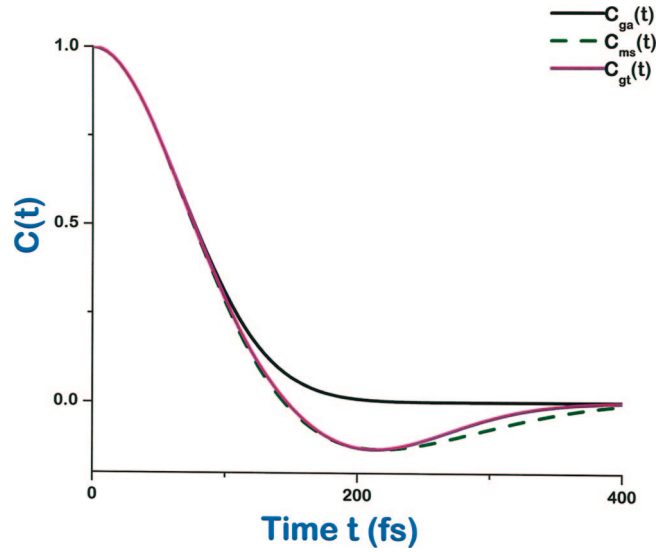

Figure 3. Similar faf's with qualitatively different wing functions. The model faf's $C_{gt}(t) = \exp[-{}^1/_2(t/\tau)^2] + a(t/\tau)^6 \exp[-{}^1/_2(t/\sigma)^2]$ (lower solid line) and $C_{ms}(t) = \cos(t/\sqrt{2}\tau)\ \mathrm{sech}(t/\sqrt{2}\tau)$ (dashed line) nearly coincide up to $t \cong 230$ fs. However, they separate as $t \to \infty$, exhibiting, respectively, short-range (Gaussian-like) and long-range (exponential-like) long time fall offs. These differences in range result in incompatible Gaussian and exponential wing functions from, respectively, $C_{gt}(t)$ and $C_{ms}(t)$, namely,[7] $\lim_{\omega\to\infty} \beta_{gt}(\omega) = \beta_{ga}(\omega) = [(\langle \mathscr{V}^2\rangle_0/k_BT)(\pi/2)^{1/2}\tau \exp(-{}^1/_2\omega^2\tau^2)]$ and $\lim_{\omega\to\infty} \beta_{ms}(\omega) = \{(\langle \mathscr{V}^2\rangle_0/k_BT)\sqrt{2}\pi\tau \exp[(-\pi\omega\tau)/\sqrt{2}] \cos(\pi/2)\}$. Additionally, $C_{ga}(t)$ of eq 2.4 is plotted (top solid line) to show the Gaussian-like character of the head parts of $C_{gt}(t)$ and $C_{ms}(t)$. The plot parameters are those of eq 2.10 and $a = 2.67 \times 10^{-3}$ and $\sigma = 1.30\tau$.

TABLE 2: (A) Normalized faf's $C_{ga}(t)$ and $C_{se}(t)$ Found from eqs 2.4 and 2.5 for the $t \leq 200$ fs Head Region, Where $C_{ga}(t) \approx C_{se}(t)$; (B) Same as Part A except for the $t > 200$ fs Tail Region, Where $C_{se}(t) \gg C_{ga}(t)$

t (fs)	$C_{ga}(t)$	$C_{se}(t)$
	(A)	
0	1.00	1.00
20	0.95	0.95
40	0.83	0.84
60	0.65	0.69
80	0.47	0.54
100	0.31	0.41
120	0.18	0.31
140	0.10	0.23
160	0.048	0.17
180	0.020	0.12
200	0.0088	0.092
	(B)	
250	6.13×10^{-4}	0.043
300	2.37×10^{-5}	0.020
350	5.06×10^{-7}	0.0092
400	5.98×10^{-9}	0.0043
450	3.91×10^{-11}	0.0020
500	1.42×10^{-13}	9.13×10^{-4}
600	3.14×10^{-19}	1.96×10^{-4}
700	6.55×10^{-26}	4.21×10^{-5}
800	1.28×10^{-33}	9.03×10^{-6}
1000	4.02×10^{-52}	4.16×10^{-7}

(1) Faf's whose short time "heads" dominate their wing functions yield physical high frequency behavior and thus meaningful (although not necessarily highly accurate) T_1's.

(2) Faf's whose long time "tails" dominate their wing functions yield unphysical high frequency behavior and T_1's which can be grossly erroneous.

(The precise statements of conditions 1 and 2 are given in ref 7.)

Loosely stated, physical and unphysical faf's have, respectively, short-range and long-range forms for $\lim_{t\to\infty} C(t)$. Thus, for example, from Figure 3, the $t \to \infty$ form of the physical faf $C_{gt}(t)$ is Gaussian-like, while that of the unphysical faf $C_{ms}(t)$ is exponential-like.

As noted, we have elsewhere[7] derived conditions 1 and 2 in a manner we believe is as rigorous and general as is possible. This rigor and generality, however, results in an involved analysis. Thus, we thought it worthwhile to publish a simplified treatment, which both captures the essence of our method and also is easy to grasp.

This simplified treatment comprises the content of this paper. It differs from our general analysis[7] mainly as follows.

(1) We restrict generality by limiting ourselves to model faf's $C_M(t)$ derived *solely* from the short time form of $C(t)$. Consequently, the long time forms, or tails, of such faf's are artifactual. Thus, any wing function dominated by these tails is also artifactual. Thus, for these faf's, condition 2 is nearly self-evident, and thus does not require further proof.

(2) In order for the general treatment to apply to all mathematically acceptable faf's,[8] it cannot presume any specific functional form for the faf's. This feature significantly complicates the analysis.

The present treatment applies only to the two model faf's $C_{ga}(t)$ and $C_{se}(t)$ of Figure 2. Moreover, these faf's and their Fourier transforms are known analytically, features which greatly simplify our analysis.

(3) Here, we bypass refractory numerical evaluations of high frequency Fourier integrals. Instead, we analyze these integrals qualitatively using graphs.

Finally, we have chosen to first study $C_{ga}(t)$ and $C_{se}(t)$, since these are the simplest model faf's which predict, respectively, Gaussian and exponential wing functions. Thus, the problem dealt with here is the simplest for which the wing function issues arise.

The plan of this paper is as follows. In section II, we develop $C_{ga}(t)$ and $C_{se}(t)$ from the exact short time expansion of $C(t)$. We also give the forms of their frequency spectra and wing functions. We note in section III that $C_{ga}(t)$ has a head dominated wing function and thus is a meaningful model for VER. Also, in section III, we show graphically that $C_{se}(t)$ has a tail dominated wing function and thus is unphysical for VER. In section IV, we summarize and discuss our work.

Finally, throughout this paper, we will use the following definitions of the frequency spectrum $\rho(\omega)$ of $C(t)$ and the friction kernel $\beta(\omega)$:

$$\rho(\omega) = \int_0^\infty \cos \omega t\, C(t)\, \mathrm{d}t \tag{1.3}$$

and

$$\beta(\omega) = \frac{\langle \tilde{\mathscr{F}}^2 \rangle_0}{k_B T}\rho(\omega) = \frac{1}{k_B T}\int_0^\infty \cos \omega t \langle \dot{\tilde{\mathscr{F}}}(t), \tilde{\mathscr{F}} \rangle_0 \, \mathrm{d}t \tag{1.4}$$

II. The Model faf's $C_{ga}(t)$ and $C_{se}(t)$

We start our analysis with the exact McLaurin series for a classical faf $C(t)$. From eq 1.2, this series is even in t and takes the form

$$C(t) = 1 - \frac{1}{2!}\frac{\langle [\dot{\tilde{\mathscr{F}}}]^2 \rangle_0 t^2}{\langle \tilde{\mathscr{F}}^2 \rangle_0} + \ldots + (-1)^{n/2}\frac{1}{n!}\frac{\langle [\tilde{\mathscr{F}}^{(n/2)}]^2 \rangle_0}{\langle \tilde{\mathscr{F}}^2 \rangle_0} t^n + \ldots \tag{2.1}$$

where n is an even integer.

To be applied, eq 2.1 must, of course, be terminated at some finite n. Our analysis here is based on the simplest $n = 2$ termination, which is the *short time approximation*

$$C_2(t) = 1 - {}^1\!/_2 \frac{t^2}{\tau^2} \tag{2.2}$$

where the decay time τ is

$$\tau \equiv \left[\frac{\langle \tilde{\mathscr{F}}^2 \rangle_0}{\langle \dot{\tilde{\mathscr{F}}}^2 \rangle_0}\right]^{1/2} \tag{2.3}$$

However, $C_2(t)$ is not a viable approximation to $C(t)$. For VER, as an example, eqs 2.2, 1.1, 1.3, and 1.4 yield the absurd result that $T_1 = \infty$. The problem, of course, is that $C_2(t)$ and $C(t)$ coincide only for very short times and then rapidly diverge with $\lim_{t\to\infty} C_2(t) = -\infty$ and $\lim_{t\to\infty} C(t) = 0$.

However, viable approximations to $C(t)$ may be developed from $C_2(t)$, by replacing the latter with an *extrapolating model faf* $C_M(t)$, built from the elements in eq 2.2. A valid model faf must reproduce $C_2(t)$ for small t but correctly vanish as $t \to \infty$, and also conform to additional mathematical conditions.[8]

Many such model faf's may exist. Here, however, we will deal with only $C_{ga}(t)$ and $C_{se}(t)$ of Figure 2, since, as noted, these are prototypical for the basic Gaussian and exponential wing types.

The forms of $C_{ga}(t)$ and $C_{se}(t)$ are

$$C_{ga}(t) = \exp\left[-\frac{1}{2}({}^t\!/_\tau)^2\right] \tag{2.4}$$

and[9]

$$C_{se}(t) = \mathrm{sech}({}^t\!/_\tau) \tag{2.5}$$

The model faf's $C_{ga}(t)$ and $C_{se}(t)$ as required coincide with each other and with $C_2(t)$ to order t^2 and vanish as $t \to \infty$.

The corresponding frequency spectra $\rho_{ga}(\omega)$ and $\rho_{se}(\omega)$ follow from eqs 2.4, 2.5, and 1.3 as

$$\rho_{ga}(\omega) = \left(\frac{\pi}{2}\right)^{1/2}\tau \exp\left(-\frac{1}{2}\omega^2\tau^2\right) \tag{2.6}$$

and[10a]

$$\rho_{se}(\omega) = \frac{\pi\tau}{2}\,\mathrm{sech}\left(\frac{\pi\omega\tau}{2}\right) \tag{2.7}$$

Note our model faf's indeed have, respectively, Gaussian and exponential wing functions, since from eqs 1.4, 2.6, and 2.7 these wing functions are

$$\lim_{\omega\to\infty}\beta_{ga}(\omega)=\frac{\langle\tilde{\mathscr{F}}^2\rangle_0}{k_BT}\left(\frac{\pi}{2}\right)^{1/2}\tau\exp\left(-\frac{1}{2}\omega^2\tau^2\right),\quad\text{Gaussian wings}\qquad(2.8)$$

and

$$\lim_{\omega\to\infty}\beta_{se}(\omega)=\frac{\langle\tilde{\mathscr{F}}^2\rangle_0}{k_BT}\pi\tau\exp\left(-\frac{\pi\omega\tau}{2}\right),\quad\text{Exponential wings}\qquad(2.9)$$

Finally, the plots and tables of this paper are developed from eqs 1.4 and 2.4−2.7 using the following representative[11] values for the parameters $\langle\tilde{\mathscr{F}}^2\rangle_0$ and τ

$$\frac{\langle\tilde{\mathscr{F}}^2\rangle_0}{k_BT}=200.0\ \text{ps}^{-2}\quad\text{and}\quad\tau=65.0\ \text{fs}\qquad(2.10)$$

Next, we quantitatively reexpress the validity conditions 1 and 2 for a model faf $C_M(t)$. Thus, we must split $C_M(t)$ into head $C_{M,H}(t)$ and tail $C_{M,T}(t)$ parts. This splitting must conform to the following requirements:

(i) $C_M(t)=C_{M,H}(t)+C_{M,T}(t)$

(ii) $C_{M,H}(t)\xrightarrow{t\to0}C_M(t)$ and $C_{M,H}(t)\xrightarrow{t\to\infty}0$

(iii) $C_{M,T}(t)\xrightarrow{t\to0}0$ and $C_{M,T}(t)\xrightarrow{t\to\infty}C_M(t)$

Theoretically based splitting algorithms are noted elsewhere.[7] For our qualitative purposes, however, we may merely choose a time t^* and then define $C_{M,H(T)}(t)$ by (i) $C_{M,H}(t\le t^*)=C_M(t)$ and $C_{M,H}(t>t^*)=0$ and (ii) $C_{M,T}(t\le t^*)=0$ and $C_{M,T}(t>t^*)=C_M(t)$. For the model faf's $C_{ga}(t)$ and $C_{se}(t)$, a satisfactory choice of t^* is 200 fs,[12] as is clear from Figure 2.

Given the comments, validity conditions 1 and 2 may be recast for any model faf $C_M(t)$ as follows.

(1) If

$$\lim_{\omega\to\infty}\int_0^{t^*}C_M(t)\cos\omega t\,dt\gg\lim_{\omega\to\infty}\int_{t^*}^{\infty}C_M\cos\omega t\,dt,\quad\textit{then } C_M(t)\textit{ is physical for VER}\qquad(2.11a)$$

(2) If

$$\lim_{\omega\to\infty}\int_{t^*}^{\infty}C_M(t)\cos\omega t\gg\lim_{\omega\to\infty}\int_0^{t^*}C_M(t)\cos\omega t\,dt,\quad\textit{then } C_M(t)\textit{ is unphysical for VER}\qquad(2.11b)$$

Returning to $C_{ga}(t)$ and $C_{se}(t)$, we have from eqs 2.4 and 2.5 that[13]

$$\lim_{t\to\infty}C_{ga}(t)=\exp[-{}^1/_2(t/\tau)^2]\qquad(2.12)$$

and

$$\lim_{t\to\infty}C_{se}(t)=2\exp[-t/\tau]\qquad(2.13)$$

TABLE 3: (A) Normalized Frequency Spectra ga(ω) and se(ω) of, Respectively, $C_{ga}(t)$ and $C_{se}(t)$ Found from eqs 3.2 and 3.3 for the $\tilde{\omega}\lesssim 200\ \text{cm}^{-1}$ Low Frequency Regime, Where ga(ω) ≈ se(ω); (B) Same as Part A except for the $\tilde{\omega}\gtrsim 200\ \text{cm}^{-1}$ High Frequency Regime, Where se(ω) ≫ ga(ω)

ω (fs^{-1})	ϖ (cm^{-1})	ga(ω)	se(ω)
		(A)	
0	0	1.00	1.00
0.004	21.24	0.97	0.92
0.008	42.47	0.87	0.74
0.012	63.71	0.74	0.54
0.016	84.94	0.58	0.38
0.02	106.18	0.43	0.26
0.024	127.41	0.30	0.17
0.028	148.65	0.19	0.11
0.032	169.88	0.11	0.076
0.036	191.12	0.065	0.050
0.04	212.35	0.034	0.034
		(B)	
0.042	222.97	0.024	0.027
0.05	265.44	0.0051	0.012
0.07	371.62	3.20×10^{-5}	0.0016
0.1	530.88	6.69×10^{-10}	7.36×10^{-5}
0.15	796.33	2.28×10^{-21}	4.46×10^{-7}
0.2	1061.77	2.00×10^{-37}	2.71×10^{-9}
0.25	1327.21	4.57×10^{-58}	1.64×10^{-11}
0.3	1592.65	2.69×10^{-83}	9.96×10^{-14}
0.35	1858.09	0.41×10^{-112}	6.04×10^{-16}
0.4	2123.53	00.16×10^{-146}	3.67×10^{-18}

Thus, $C_{ga}(t)$ is a short-range function with rapid Gaussian decay, while $C_{se}(t)$ is a long-range function with slow exponential decay. Consequently, in accord with the comments about range in the Introduction, we expect that $C_{ga}(t)$ conforms to eq 2.11a and thus is physical for VER and that $C_{se}(t)$ conforms to eq 2.11b and thus is unphysical for VER. We next show that this is indeed true.

III. Elimination of $C_{se}(t)$

Given the short range of $C_{ga}(t)$, from Figure 2, it is evident that $C_{ga}(t)$ conforms to eq 2.11a and thus is a possible model for VER. In the rest of this section, we eliminate $C_{se}(t)$ of eq 2.5 as a possible model for VER by proving the following.

eq 2.11b, with $\lim_{\omega\to\infty}$ *interpreted as* $\tilde{\omega}\gtrsim$ *200 cm^{-1}, holds for* $C_{se}(t)$ (3.1)

We next give three distinct arguments for eq 3.1. The first is based in Tables 2 and 3.

A. The Evidence of Tables 2 and 3. Parts A and B of Table 2 compare $C_{ga}(t)$ and $C_{se}(t)$ for, respectively, the $t\le t^*=200$ fs head region and the $t>t^*$ tail region. Correspondingly, parts A and B of Table 3 compare the normalized frequency spectra

$$\text{ga}(\omega)\equiv\rho_{ga}{}^{-1}(0)\,\rho_{ga}(\omega)=\exp\left[-\frac{1}{2}\omega^2\tau^2\right]\qquad(3.2)$$

and

$$\text{se}(\omega)\equiv\rho_{se}{}^{-1}(0)\,\rho_{se}(\omega)=\text{sech}\left(\frac{\pi\omega\tau}{2}\right)\qquad(3.3)$$

for, respectively, the $\tilde{\omega}\lesssim 200\ \text{cm}^{-1}$ low frequency regime and the $\tilde{\omega}\gtrsim 200\ \text{cm}^{-1}$ high frequency or wing function regime.

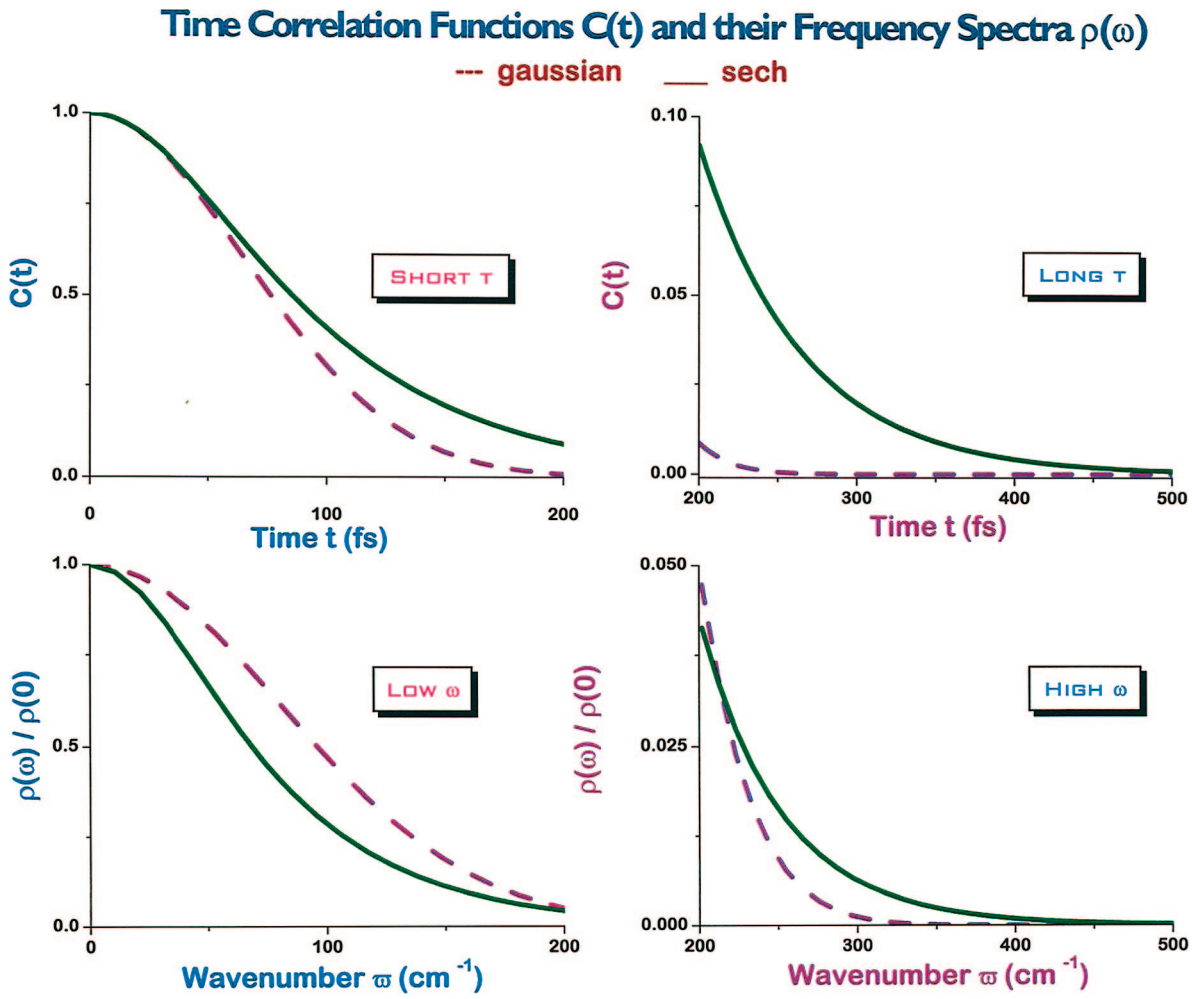

Figure 4. Breakdown of Fourier complementarity for the model faf's. Top panels: Normalized faf's $C_{ga}(t)$ (dashed curves) and $C_{se}(t)$ (solid curves) of eqs 2.4 and 2.5 in the short time (left panel) and long time (right panel) regimes. Bottom panels: Corresponding normalized frequency spectra $\rho_{ga}(\omega)/\rho_{ga}(0)$ (dashed curves) and $\rho_{se}(\omega)/\rho_{se}(0)$ (solid curves) of eqs 3.2 and 3.3 in the low frequency (left panel) and high frequency (right panel) regimes. The top left and bottom left panels show Fourier complementarity, indicating that the low frequency form of $\rho_{se}(\omega)$ is dominated by the short time head part of $C_{se}(t)$. In contrast, the top left and bottom right panels show Fourier *non*complementarity, indicating that the high frequency wings of $\rho_{se}(\omega)$ derive from the long time tail part of $C_{se}(t)$.

Table 2A shows that for the head region $C_{ga}(t) \approx C_{se}(t)$ with the faf's never differing by more than an order of magnitude. Moreover, from Figure 2, in the head region, the slope of $C_{ga}(t)$ is greater than that of $C_{se}(t)$. Thus, if the head region dominated ga(ω) and se(ω), one would expect ga(ω) $\gtrsim$ se(ω). From Table 3A, this is, in fact, true in the low ω regime. In striking contrast, Table 3B shows (in accord with Table 1) that in the high ω regime se(ω) $\gg$ ga(ω), with the frequency spectra differing by tens of orders of magnitude for $\tilde{\omega}$'s typical of common molecules like N_2 and O_2.

Thus, it is not plausible that ga(ω) and se(ω) of Table 3B both derive from the head parts of $C_{ga}(t)$ and $C_{se}(t)$ in Table 2A. We will see shortly that at high ω se(ω) actually derives from the *tail part* of $C_{se}(t)$ of Table 2B, in accord with eq 3.1.

The above is a plausibility argument. We next turn to more rigorous and penetrating arguments.

We start by applying a simple but powerful property of Fourier transforms. Namely, the time and frequency domain forms of a function f, respectively $f(t)$ and $f(\omega)$, have the following complementary behavior.

If as t increases f(t) decays slowly, then as ω increases f(ω) decays rapidly and vice versa (3.4)

B. High Frequency Breakdown of Fourier Complementarity. Consider Figure 4 which is a four-paneled plot of the data in Tables 2 and 3. For example, the top left panel plots the data in Table 2A. Notice that Table 2A shows that in the head region $C_{se}(t)$ decays *more slowly* than $C_{ga}(t)$. Consequently, from eq 3.4, $\rho_{se}(\omega)$ should decay *more rapidly* than $\rho_{ga}(\omega)$, if these frequency spectra are dominated by the head parts $C_{ga,H}(t)$ and $C_{se,H}(t)$. From the top and bottom left panels of Figure 4, this predicted complementarity holds in the low frequency regime.

However, comparing the top left and bottom right panels shows that this Fourier complementarity breaks down at high frequency. Namely, at high ω, $\rho_{se}(\omega)$ decays more slowly not more rapidly than $\rho_{ga}(\omega)$.

The only explanation is that, at high ω, $\rho_{se}(\omega)$ is determined by the tail part $C_{se,T}(t)$ not the head part $C_{se,H}(t)$. This result provides a second validation of eq 3.1.

Next, we pinpoint the origin of the proceeding results via a graphical analysis of the Fourier integral of eq 1.3, specialized to our models. This analysis identifies the time domains which dominate this integral for both low and high frequencies.

C. Graphical Analysis of the Fourier Integrands. Specifically, we graphically compare the low and high frequency forms of the Fourier integrands for $\rho_{se}(\omega)$ and $\rho_{ga}(\omega)$, respectively,

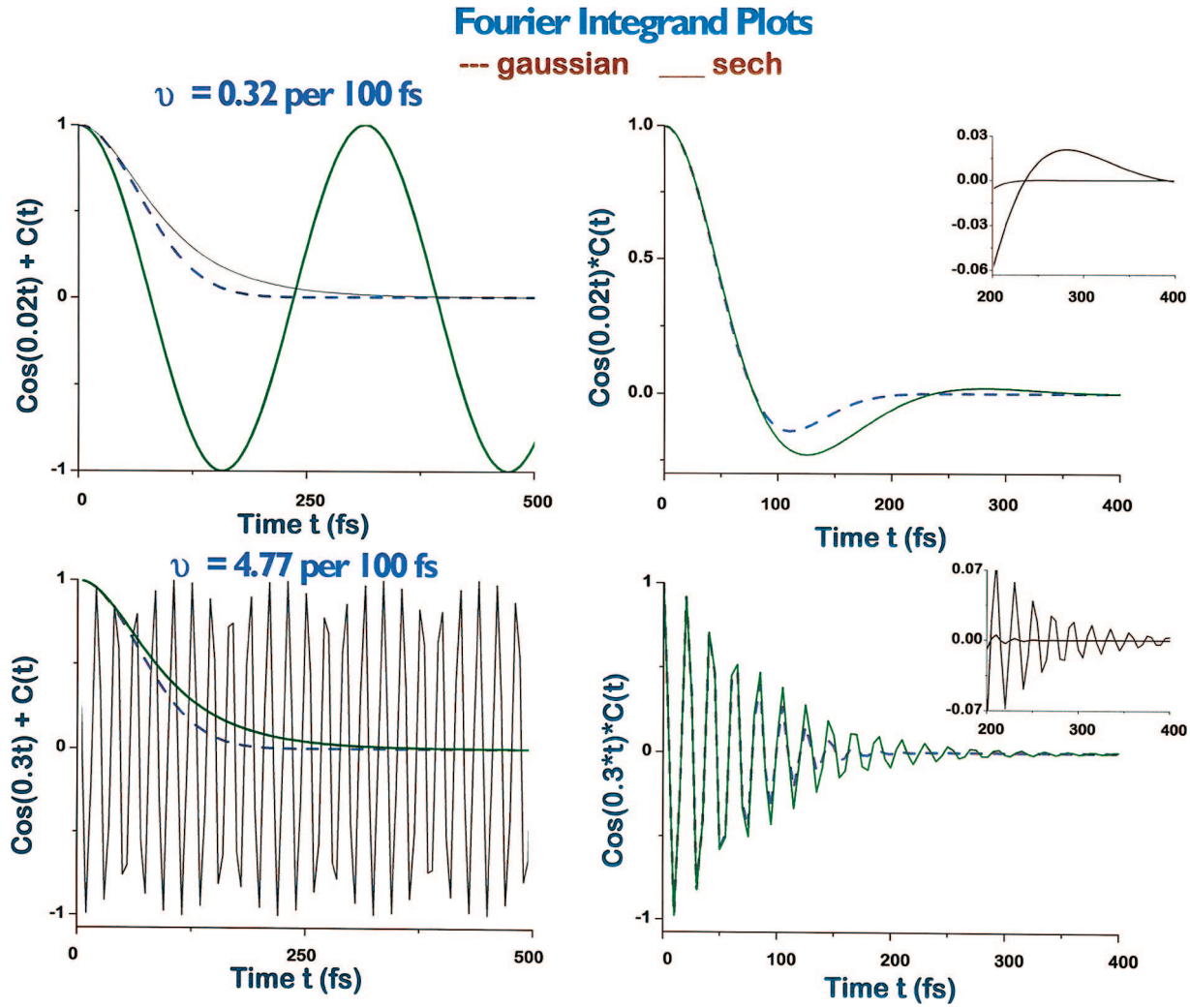

Figure 5. Fourier integrands for $C_{ga}(t)$ and $C_{se}(t)$. Left panels: Components $C_{se}(t)$ (solid curves), $C_{ga}(t)$ (dashed curves), and cos ωt (solid curves) of the Fourier integrands in eq 1.3 for (top panel) low frequency $\nu = \omega/2\pi = 0.32$ per 100 fs ($\tilde{\omega} = 106.18$ cm^{-1}) and (bottom panel) high frequency $\nu = 4.77$ per 100 fs ($\tilde{\omega} = 1592.65$ cm^{-1}). Right panels: Fourier integrands cos ωt $C_{se}(t)$ (solid curves) and cos ωt $C_{ga}(t)$ (dashed curves) for (top panel) $\nu = 0.32$ per 100 fs and (bottom panel) $\nu = 4.77$ per 100 fs. The right panel plots show that cancelation of the head contributions to the Fourier integrals in eq 1.3 is mild at low frequency but virtually complete at high frequencies, again implying that the high frequency wings of $\rho_{se}(\omega)$ are dominated by the tail of $C_{se}(t)$ (see inset plot in the bottom right panel).

cos ωt $C_{se}(t)$ and cos ωt $C_{ga}(t)$. We find that these two forms are radically different, and that, moreover, the differences give rise to the qualitatively disparate low and high frequency behaviors seen in Figure 4.

Our main points are summarized in the four-paneled plot in Figure 5. In the two left-hand panels, we plot the components cos ωt and $C_{se}(t)$ and $C_{ga}(t)$ of the Fourier integrands, and in the two right-hand panels, we plot the integrands themselves. The plots in the top and bottom panels pertain, respectively, to the representative low and high frequency wavenumbers $\tilde{\omega} =$ 106.18 cm^{-1} and $\tilde{\omega} = 1592.65$ cm^{-1}.

Fourier integrand plots like those of Figure 5 are useful, since they provide quick qualitative assessments of the magnitudes of *partial contributions*

$$\rho_{[t_1,t_2]}(\omega) \equiv \int_{t_1}^{t_2} \rho(\omega) \cos \omega t \, C(t) \, dt \qquad (3.5)$$

to spectra $\rho(\omega)$ from subintervals $[t_1, t_2]$ of the full integration interval $[0,\infty]$ of eq 1.3, and, especially, can identify a subinterval which dominates $\rho(\omega)$. This follows since $\rho_{[t_1,t_2]}(\omega)$ can be estimated visually from a Fourier integrand plot of $C(t)$ cos ωt, since by eq 3.5 it is just the partial area under that plot enclosed by $[t_1, t_2]$.

These notions are pertinent to our faf validity conditions, eqs 2.11a, since these are comparisons of distinct partial contributions. Thus, our faf *invalidity* condition of eq 2.11b may be written in terms of partial contributions as

$$\rho_{[200\ \mathrm{fs},\infty]}(\omega) \gg \rho_{[0,200\ \mathrm{fs}]}(\omega) \qquad (3.6)$$

where $\omega \rightarrow \infty$ (or in practice $\tilde{\omega} \geq 200$ cm^{-1}). Equation 3.6 may be used to eliminate unphysical faf's by visual inspection of their Fourier integrand plots.

We next apply those procedures to $C_{se}(t)$ and $C_{ga}(t)$.

We will focus, in this analysis, on the canceling effects of the cos ωt oscillations, evident in Figure 5, on the Fourier integrals for $\rho_{se}(\omega)$ and $\rho_{ga}(\omega)$. The increasing destructiveness of these oscillations as ω increases of course underlies the gross decays of $\rho_{se}(\omega)$ and $\rho_{ga}(\omega)$. However, Figure 5 also reveals a more subtle effect of the oscillations. Namely, as ω increases, the time subinterval $[t_1, t_2]$ which dominates $\rho_{se}(\omega)$ (but not

$\rho_{ga}[\omega]$) *shifts* from the head to the tail subinterval. This shift underlies the disparate low and high frequency behaviors in Figure 4.

We next validate this behavior. We start with the $\tilde{\omega} < 200$ cm^{-1} low frequency regime (top panels of Figure 5).

1. Low Frequency Regime. We show that, for $\tilde{\omega} < 200$ cm^{-1}, the dominant subinterval in eq 1.3 for both $\rho_{se}(\omega)$ and $\rho_{ga}(\omega)$ is the head subinterval. That is, for $\omega < 200$ cm^{-1},

$$\rho_{[0,200\ fs]}(\omega) = \int_0^{200\ fs} C(t) \cos \omega t\, dt \gg \int_{200\ fs}^{\infty} C(t) \cos \omega t\, dt = \rho_{[200\ fs,\infty]}(\omega) \quad (3.7)$$

for both $C(t) = C_{se}(t)$ and $C_{ga}(t)$.

The origin of eq 3.7 is that the heads of $C_{se}(t)$ or $C_{ga}(t)$ have far larger amplitudes than their tails (Figure 2). This origin is most easily seen by considering the $\omega = 0$ limit.

a. The $\omega = 0$ Limit. For $\omega = 0$, the integrals in eq 3.7 reduce to the head and tail partial areas A_H and A_T under the faf's of Figure 2. (A_T for $C_{se}[t]$ is the shaded area in Figure 2.) Thus, for $\omega = 0$, eq 3.7 reduces to

$$A_H = \int_0^{200\ fs} C(t)\, dt \gg \int_{200\ fs}^{\infty} C(t)\, dt = A_T \quad (3.8)$$

Visual inspection of Figure 2 shows that for both model faf's $A_H \gg A_T$, confirming eq 3.8.

This graphical argument may be checked by analytic integration.[10b] This integration yields that for $C_{se}(t)$ and $C_{ga}(t)$ the head areas A_H are, respectively, 94.1 and 99.9% of the total areas under the $C(t)$ curves in accord with eq 3.8.

b. Finite ω. The head domination of the $\rho(\omega)$'s at $\omega = 0$ persists over the whole low frequency regime, since throughout that regime the cos ωt head canceling effects are mild.

Specifically, consider the typical low frequency regime wavenumber $\tilde{\omega} = 106.18$ cm^{-1}. For this $\tilde{\omega}$, the cos ωt oscillation frequency $\nu = \omega/2\pi = 0.32$ oscillations per 100 fs. Referring to Figure 5 (top left panel) for this small ν, only 0.64 complete cos ωt cycles cover the 0−200 fs head interval. This sparse coverage suggests that at $\tilde{\omega} = 106.18$ cm^{-1} the destructive cancelation of the head contributions to $\rho(\omega)$ will be mild, and the $\omega = 0$ picture will persist qualitatively.

This expectation is borne out by the Fourier integrand plot in Figure 5 (top right panel). Visual comparison shows that the head areas dominate for both model faf's, thus validating eq 3.7 at $\tilde{\omega} = 106.18$ cm^{-1} (a validation which was checked by numerical integration[7]).

Finally, our finding of head domination of the $\rho(\omega)$'s at low ω is in accord with the following prior results.

(i) From Table 2A, $C_{se}(t)$ and $C_{ga}(t)$ have similar head magnitudes, while, from Table 3A, se(ω) and ga(ω) have similar low ω magnitudes.

(ii) From Figure 4, Fourier complementarity holds between the head parts of $C_{se}(t)$ and $C_{ga}(t)$ and the low ω parts of se(ω) and ga(ω).

We now turn to the $\tilde{\omega} \geq 200$ cm^{-1} high frequency regime (bottom panels of Figure 5).

2. High Frequency Regime. We next show that for $\tilde{\omega} > 200$ cm^{-1} the tail part of $C_{se}(t)$ becomes dominant in eq 1.3 and that the following condition, equivalent to eq 2.11b, thus holds

$$\rho_{se[200\ fs,\infty]}(\omega) = \int_{200\ fs}^{\infty} C_{se}(t) \cos \omega t\, dt \gg \int_0^{200\ fs} C_{se}(t) \cos \omega t\, dt = \rho_{se[0,200\ fs]}(\omega) \quad (3.9)$$

Tail dominance occurs due to the long (exponential) range of $C_{se,T}(t)$, evident in eq 2.13. Due to this long range, the contributions of $C_{se,T}(t)$ to eq 1.3 accumulate over many more cos ωt cycles than do those of $C_{se,H}(t)$, and as a result, as $\omega \rightarrow \infty$, $C_{se,T}(t)$ swamps the short-range $C_{se,H}(t)$ in eq 1.3, even though in decay rate $C_{se,T}(t) \ll C_{se,H}(t)$. (This behavior does not conflict with eq 3.4, since eq 3.4 can only compare functions of similar range.)

To go further, we next examine head cancelations by cos ωt oscillations.

a. Head Cancelations at High ω. Consider the typical high ω wavenumber $\tilde{\omega} = 1592.65$ cm^{-1}. For this $\tilde{\omega}$, the cos ωt oscillation frequency is $\nu = 4.77$ oscillations per 100 fs. Referring to Figure 5 (bottom left panel) for this large ν, more than 9.5 complete cos ωt cycles cover the 0−200 fs head region. Due to this dense coverage, the head parts of the corresponding Fourier integrand plots (lower right panel of Figure 5) rapidly oscillate between positive and negative values, and thus, the head contributions to $\rho_{se(ga)}(\omega)$ are massively canceled.

We next examine these head cancelations quantitatively.

We start with $C_{ga}(t)$ because its high ω behavior is especially simple, since from Figure 2 or Table 2B $C_{ga,T}(t) \cong 0$. Consequently, eq 1.3 for $\rho_{ga}(\omega)$ may be approximated by

$$\rho_{ga}(\omega) = \int_0^{\infty} \cos \omega t\, C_{ga}(t)\, dt \simeq \int_0^{200\ fs} \cos \omega t\, C_{ga}(t)\, dt \quad (3.10)$$

Hence, from eqs 2.6, 3.2, and 3.10,

$$\textit{the head contribution to } \rho_{ga}(\omega) \cong \rho_{ga}(\omega) = \left(\frac{\pi}{2}\right)^{1/2} \tau ga(\omega) \quad (3.11)$$

Equation 3.11 permits that the head contribution to $\rho_{ga}(\omega)$ be estimated from eq 3.2 or Table 3B. For $\tilde{\omega} = 1592.65$ cm^{-1}, Table 3B gives (using $\tau = 65.0$ fs)

$$\textit{head contribution to } \rho_{ga}(\omega) \cong 2.19 \times 10^{-81}\ fs \quad \text{for } \tilde{\omega} = 1592.65\ cm^{-1} \quad (3.12)$$

This miniscule value is in accord with the massive head cancelations evident from Figure 5.

Next, we turn to $C_{se}(t)$. First, as noted earlier, the heads of $C_{se}(t)$ and $C_{ga}(t)$ are similar in magnitude and slope. Thus, for both faf's, the high ω Fourier integrands (bottom right panel in Figure 5) are similar in the head region. This suggest the rough estimate

$$\textit{head contribution to } \rho_{se}(\omega) \cong 2.19 \times 10^{-81}\ fs \quad \text{for } \tilde{\omega} = 1592.65\ cm^{-1} \quad (3.13)$$

Additionally the full value of $\rho_{se}(\omega)$ is from eqs 2.7 and 3.3 and Table 3B

$$\rho_{se}(\omega) = \frac{\pi\tau}{2}\mathrm{se}(\omega) = 1.02 \times 10^{-11}\ \mathrm{fs} \quad \text{for } \tilde{\omega} = 1592.65\ \mathrm{cm}^{-1} \qquad (3.14)$$

Comparison of eqs 3.13 and 3.14 suggests that at high ω the head contribution to $\rho_{se}(\omega)$ is negligible and that therefore

in the high ω regime $\rho_{se}(\omega)$ is solely determined by the $t \geq$ 200 fs tail part of $C_{se}(t)$ (3.15)

Equation 3.15 is in accord with eq 3.1, and thus eliminates $C_{se}(t)$ for VER.

However, one might object to eq 3.13 and hence eq 3.15, since from Figure 2 $C_{se,H}(t)$ and $C_{ga,H}(t)$ differ for $t \gtrsim 50$ fs in both magnitude and slope. The magnitude differences are of order unity and, thus, are far too small to upset the argument for eq 3.15. Moreover, the slope differences actually strengthen the conclusion of eq 3.15. Namely, from Figure 2, the slope of $C_{se,H}(t)$ is less than that of $C_{ga,H}(t)$. Thus, from eq 3.4, the slope differences decrease the head contribution to $\rho_{se}(\omega)$ from the estimate of eq 3.13. This decrease can be many orders of magnitude,[7] and thus, eq 3.13 should be replaced by

head contribution to $\rho_{se}(\omega) \ll$ *head contributions to* $\rho_{ga}(\omega) \cong 2.19 \times 10^{-81}$ fs (3.16)

Equations 3.14 and 3.16 again yield our main conclusion eq 3.15.

IV. Summary and Discussion

All modern theories of solute VER[2,4,5] require as input a form for the *wing function* $\lim_{\omega\to\infty}\beta(\omega)$ depicted in Figure 1. Moreover, if an unrealistic model wing function is inputed, as illustrated by Table 1, theoretical T_1's in error by tens of orders of magnitude can result. Thus, a key problem in VER theory is to find a way to identify and eliminate qualitatively unrealistic wing function models.

Seemingly, this problem may be dealt with straightforwardly by a molecular dynamics (MD) determination of the exact wing function, followed by comparison of exact and model forms. Such a determination would require an MD simulation of the faf $C(t)$ followed by a Fourier transform.[4b,14] However, several problems, all stemming from the $\omega \to \infty$ requirement, render this "straightforward" procedure anything but easy. Most obviously, the wing function's minute amplitude and highly oscillatory integrand renders it very difficult to meaningfully evaluate from a $C(t)$ contaminated by statistical error and, moreover, computed out only to a finite time.[15]

Motivated by such considerations, here and elsewhere,[7] we have outlined a theoretical analysis of the wing function problem. Our central results are shown by eq 2.11a. These are conditions for the acceptability of a model faf $C_M(t)$ for VER. In brief, eq 2.11a accepts (rejects) $C_M(t)$'s whose wing functions are dominated by their short time heads (long time tails).

We next discuss three points which perhaps need further clarification.

(1) The sharp and somewhat arbitrary divide at the $t^* \approx 200$ fs of $C_{ga}(t)$ and $C_{se}(t)$ into head and tail parts, evident in Figure 2, can be replaced by more rigorous partition[7] and thus does not negate our main conclusions. Relatedly, note that Figure 3, which is free of divides, shows unambiguously that the exponential wings yielded by $C_{ms}(t)$ derive from its $t \gtrsim 230$ fs tail.

(2) Equation 2.11a as derived here apply only to faf's built *solely* from the parameters in eq 2.1, that is, from exact short time dynamics. Nonetheless, our results here have useful applications. For example, eq 2.1 is the most convenient basis for building model faf's,[2] and eqs 2.11a permit one to test such model faf's for validity.

However, because of short the time dynamics limitation, the present work leaves open two important and related questions: (a) Are there model faf's, built from *elements additional to short time parameters*, which have *both* tail dominated wing functions and which are *also* physical for VER? (b) The basis of eq 2.11b is so far purely mathematical.[13] Is there a *physical basis* for eq 2.11b? Such a basis would make eq 2.11b valid for all faf's, and eliminate the possibility of (a).

In fact, there is such a physical basis. It emerged in the earliest treatments of vibrational energy transfer (VET),[16,17] for example, that of Landau and Teller.[16] This work showed that VET derives from *short time dynamics*. When transcribed to liquids (from gases), the arguments of these early workers may be paraphrased as follows. Those collisions strongly influenced by the steep repulsive part of the solute−solvent potential dominate rates. This is because, for steep repulsive wall collisions, the vibrational forces change very rapidly and thus such collisions dominate the high frequency vibrational force Fourier components which induce VER. Additionally, due to the short range of repulsive forces, the collisions in question are short time processes.

Thus, the physics of VER is the true basis for the link between short times and high frequencies.

Others have similarly made this link.

For example, long ago, Herzfeld[18] commented as follows. *"The autocorrelation function (faf) is very sharply dependent on... the relative velocity.... For low velocities, the duration of a collision... is so long, i.e. the autocorrelation function so broad, that the power spectrum contains only negligible components at (the relaxing molecule) frequency ω. For the high velocity collisions, the autocorrelation function contracts and the high frequency components (of the friction kernel) increase (inducing VER)."*

More recently, Simpson and co-workers[14] have made similar comments concerning their MD simulation results. *"At large values of* $\Delta\tilde{v}$ (corresponding to our high ω regime) *the very* **short time characteristics** *of the correlation function (faf) are reflected in the Fourier transform and hence* k_L (our T_1^{-1})."

Very recently, Stratt and co-workers,[19] in the context of their molecular theory of VER, have repeatedly stressed the short time scale/high frequency link. For example, Larsen and Stratt[19a] state (on their p 1038): *"... (If we) then ask where we should expect the major high frequency components of the correlation function to arise...this analysis will immediately lead us to look at the* **short-time scattering dynamics** *of the solute and a single crucial solvent partner.* As a second example on p 1039 *"...this same conceptual distinction ought to continue to operate at* **short times - and therefore at high frequencies...**"

The short time/high frequency link is established definitively in ref 7. There we show that the empirical

correlation between gas and liquid phase VER rates[20] (which provides the experimental basis for the isolated binary collision model[1a]) emerges from theory only if the wing function is dominated by the relaxing molecules shortest time dynamics.

(3) Finally, we wish to discuss the apparent disagreement between our results which predict Gaussian-like wing functions (since realistic faf heads are typically Gaussian-like[2a,f,4b]) and the experimental exponential energy gap laws.[21]

Actually, there may be no real disagreement, since energy gap laws have mainly been seen for solid and not liquid state processes.[21] The few MD studies of liquid phase VER,[4b,14,19a] which might suggest an exponential wing function, have not yielded $\beta(\omega)$ precisely enough and at high enough frequencies to unambiguously pin down $\lim_{\omega\to\infty}\beta(\omega)$.

More work in this area is needed.

References and Notes

(1) (a) For a comprehensive review, see: Chesnoy, J.; Gale, G. M. *Ann. Phys. Fr.* **1984**, *9*, 893. (b) For an extensive list of more recent references, see refs 2d and 2f.

(2) (a) Adelman, S. A.; Stote, R. H. *J. Chem. Phys.* **1988**, *88*, 4397, 4415. (b) Adelman, S. A.; Muralidhar, R.; Stote, R. H. *J. Chem. Phys.* **1991**, *95*, 2738. (c) Adelman, S. A.; Ravi, R.; Muralidhar, R.; Stote, R. H. *Adv. Chem. Phys.* **1993**, *84*, 73. (d) Adelman, S. A.; Stote, R. H.; Muralidhar, R. *J. Chem. Phys.* **1993**, *99*, 1320. (e) Adelman, S. A.; Muralidhar, R.; Stote, R. H. *J. Chem. Phys.* **1993**, *99*, 1333. (f) Miller, D. W.; Adelman, S. A. *J. Chem. Phys.* **2002**, *117*, 2672, 2688.

(3) (a) Herzberg, G. *Molecular Spectra and Molecular Structure I. Structure of Diatomic Molecules*; Van Nostrand Reinhold: New York, 1950; Table 39. (b) Wade, L. G., Jr. *Organic Chemistry*, 3rd ed.; Prentice Hall: Upper Saddle River, NJ, 1995; pp 1256−1260.

(4) An approach related to that of ref 2 has been advanced by Skinner and co-workers. See, for example:(a) Egorov, S. A.; Skinner, J. L. *J. Chem. Phys.* **1996**, *105*, 7047. (b) Everitt, K. F.; Egorov, S. A.; Skinner, J. L. *Chem. Phys.* **1998**, *235*, 115. (c) Everitt, K. F.; Skinner, J. L.; Ladanyi, B. M. *J. Chem. Phys.* **2002**, *116*, 179.

(5) (a) For other modern treatments of liquid phase VER, see, for example: Whitnell, R. M.; Wilson, K. R.; Hynes, J. T. *J. Chem. Phys.* **1992**, *96*, 5354. (b) Benjamin, I.; Whitnell, R. M. *Chem. Phys. Lett.* **1993**, *204*, 45. (c) Bruehl, M.; Hynes, J. T. *Chem. Phys.* **1993**, *175*, 205. (d) Ferrario, M.; Klein, M. L.; McDonald, I. R. *Chem. Phys. Lett.* **1993**, *213*, 537. (e) Poulsen, J.; Nymand, T. M.; Keiding, S. R. *Chem. Phys. Lett.* **2001**, *43*, 581. (f) Sibert, E. L., III; Roy, R. *J. Chem. Phys.* **2002**, *116*, 237. (e) Chorny, I.; Viecelli, J.; Benjamin, I. *J. Chem. Phys.* **2002**, *116*, 8904.

(6) For the precise meaning of eq 1.2, see: Adelman, S. A. *J. Chem. Phys.* **1984**, *81*, 2776; *Int. J. Quant. Chem. Symp.* **1987**, *21*, 199.

(7) Adelman, S. A. In preparation.

(8) For mathematical acceptability, a $C(t)$ must be even, analytic at $t = 0$, and have a nonnegative frequency spectrum.

(9) $C_{se}(t)$ is a special case of the model faf used in ref 4.

(10) Gradshteyn, I. S.; Ryzhik, I. M. *Tables of Series, Integrals, and Products*; Academic: New York, 1980. See entries (a) 2.423.4 and (b) 3.511.4.

(11) The parameters of eq 2.10 were derived by applying the methods of ref 2 to pure O_2 at thermodynamic state $T = 75.4$ K and $\rho = 2.4 \times 10^{22}$ cm^{-3}. A site−site Lennard-Jones $[O_2]_2$ potential was used with parameters $\varepsilon = 58$ K and $\sigma = 2.988$Å representative of literature values. Because of the crudity of the potential, the values of eq 2.10 are best viewed as representative for liquid phase VER, rather than realistic for O_2 VER.

(12) The choice $t^* = 200$ fs is made, since from Table 2A for $t \geqslant 200$ fs $C_{ga}(t) < 1\%\ C_{ga}(t=0)$. (The qualitative conclusions of this paper remain unchanged for any reasonable choice of t^*.).

(13) The mutually exclusive nature of eqs 2.12 and 2.13 and the fact that both are consistent with the short time approximation of eq 2.2 illustrates that eq 2.2 provides no information about the true long time behavior of $C(t)$, and that eqs 2.12 and 2.13 are artifacts of our choice of model faf's unrelated to the true long time form of $C(t)$. This observation is in accord with our comments in the Introduction about the artifactual nature of wing functions dominated by faf tails. Equation 2.11b is, of course, just a restatement of these comments. Thus, the incompatible nature of eqs 2.12 and 2.13 illustrates the basis for the faf rejection condition eq 2.11b.

(14) Andrew, J. J.; Harriss, A. P.; McDermott, D. C.; Williams, H. T.; Madden, P. A.; Simpson, C. J. S. M. *Chem. Phys.* **1989**, *139*, 369 (especially sections 4 and 5).

(15) The finite time limitation is especially insidious. This is because the extrapolating function selected to extend the MD $C(t)$ to ∞ may as $\omega \to \infty$ dominate the Fourier integral in eq 1.3, yielding a spurious wing function. This problem closely relates to the issues of Figure 3.

(16) Landau, L.; Teller, E. *Phys. Z. Sowjetunion* **1936**, *10*, 34.

(17) (a) Zener, C. *Phys. Rev.* **1931**, *37*, 556; *38*, 277. (b) Jackson, J. M.; Mott, N. F. *Proc. R. Soc. London* **1932**, *127A*, 703. (c) See, for example: Schwarz, R. N.; Slawsky, Z. I.; Herzfeld, K. F. *J. Chem. Phys.* **1952**, *20*, 1591.

(18) Herzfeld, K. F. *J. Chem. Phys.* **1962**, *36*, 3305.

(19) See, for example: (a) Larsen, R. E.; Stratt, R. M. *J. Chem. Phys.* **1999**, *110*, 1036. (b) Deng, Y. Q.; Ladanyi, B. M.; Stratt, R. M. *J. Chem. Phys.* **2002**, *117*, 10752.

(20) See Table 1 of ref 1a.

(21) See, for example: (a) Nitzan, A.; Mukamel, S.; Jortner, J. *J. Chem. Phys.* **1975**, *60*, 3929; *63*, 200. For more recent discussions, see, for example, ref 19 and also: (b) Egorov, S. A.; Skinner, J. L. *J. Chem. Phys.* **1995**, *103*, 1553; *105*, 10153.

(22) Note added in proof: After acceptance of this paper we learned that the importance of short time dynamics for VER has also been discussed by: Bagchi, B.; Biswas, R. *Adv. Chem. Phys.* **1999**, *109*, 207. Biswas, R.; Bhattacharyya, S.; Bagchi, B. *J. Chem. Phys.* **1998**, *108*, 4963.

JP806560X